Acta Mechanica Slovaca **27 (4): 62 - 74,** December **2023**
https://doi.org/10.21496/ams.2023.034

Acta Mechanica Slovaca
ISSN 1335-2393
www.actamechanica.sk

Modelling and Experimental Testing of a Solar Thermoelectric Refrigerator

Francis Onoroh [1*], Uche Paul Onochie [2], Larry Orobome Agberegha [3]

[1] Full Affiliation, Department of Mechanical Engineering, University of Lagos, Akoka, Yaba, Lagos Nigeria
[2] Full Affiliation, Department of Mechanical Engineering, Alex Ekwueme University, Ndufu Alike, Nigeria
[3] Full Affiliation, Department of Mechanical Engineering, Federal University of Petroleum Resources, Effurun, Delta state, Nigeria

Abstract: This research centered on the design, simulation and testing of a solar thermoelectric refrigerator. Mathematical models of the system were derived and solved using MATLAB to predict the performance of the refrigerator at various operating conditions of applied voltage and temperature gradients. Simulations were carried out in order to test the system's effectiveness when powered with solar energy. Simulation results of the thermoelectric refrigeration showed the heat pumping capacities of the TEC1-12706 module as 42.6W, 38.9W, 35.3W and 31.7W at temperature gradients of 5°C, 10°C, 15°C and 20°C respectively, the heat dissipation capacities of the TEC1-12706 module as 132 W, 125.3 W, 118.7 W and 112.2 W at temperature gradients of 5°C, 10°C, 15°C and 20°C respectively and the corresponding coefficient of performance as 0.468, 0.436, 0.402 and 0.368 at temperature gradients of 5°C, 10°C, 15°C and 20°C respectively. The experimental results indicated a steady decline of temperature in the refrigerated chamber from 28.7°C to 3.3°C in a time frame of three hours. Thus, solar power thermoelectric refrigerator is an alternative source of cooling as it is environmentally friendly.

Keywords: Thermoelectric refrigerator, Coefficient of Performance, Temperature gradient, Solar irradiation, Photovoltaic.

1. Introduction

Conventional refrigerators consume a lot of electricity and are not environmentally friendly. In a bid to find better alternatives, thermoelectric cooling modules were invented. Thermoelectric refrigerator uses the Peltier effect to absorb heat from an enclosed space when a direct current voltage is applied across its terminals, they are very portable and virtually noiseless; but possess low coefficient of performance compared to the vapour compression refrigerator systems.

Thermoelectric cooling design is beneficial because it reduces the number of moving parts giving room for easy repair, portability, low cost, reduced danger and easier packaging of the system and there is no need for a refrigerant which makes them eco-friendly [1][2]. A standard thermoelectric module is made up of two ceramic substrates which are the basis for the p-type and n-type bismuth telluride which is electrically connected in series and thermally connected in parallel between the plates [3][4]. Figure 1 shows the schematic of a thermoelectric cooler.

Thermoelectric modules are composed of an array of p-type and n-type semiconductors materials bounded by ceramic substances that serve as electrical insulation [6]. These semiconductors are placed electrically in series and thermally in parallel. The p-type and n-type materials are alloys of Bismuth and Tellurium [7]. The p-type semiconductors have a higher hole concentration than their electron concentration

*** Corresponding author:** Francis Onoroh, ***E-mail address:*** *fonoroh@unilag.edu.ng*

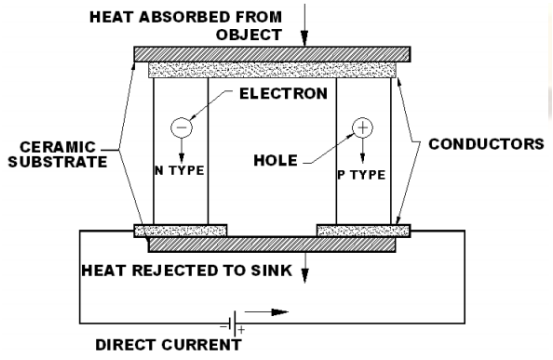

Figure 1: Thermoelectric Cooler

due to the use of doping elements which are mostly group III elements that need extra electron for bonding and hence create holes, whereas in n-type semiconductors, the reverse occurs. A pair of the p-type and n-type semiconductor elements is referred to as a couple. Figure 2 shows the constructional details of a thermoelectric modules.

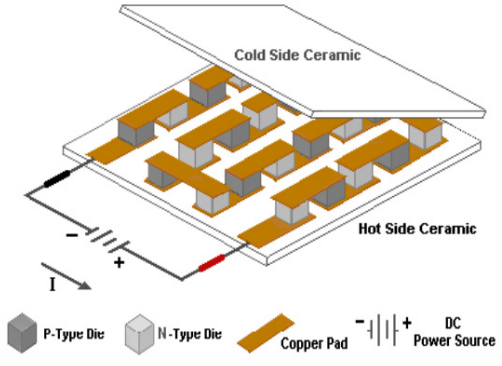

Figure 2: Construction of Thermoelectric Module [3]

When a current or voltage is applied to the Peltier module, there is a tendency for conduction electrons to complete the atomic bonds, when conduction electrons do this, they leave holes which essentially are atoms within the crystal lattice that now have local positive charges, this leads to electrons dropping into a hole and then moving to the next available hole [8]. Semiconductors are the optimum choice of material to place between the two metal conductors because of the possibility of controlling the semiconductors' charge carriers and increasing the heat pumping ability [6]. The figure of merit details out the quality and efficiency of a thermoelectric material. It is the ratio of the Seebeck coefficient to the product of the thermal conductivity and the material's electrical resistivity. Table 1 shows the figure of merit for some common thermoelectric Peltier modules.

The use of photovoltaic cells to power thermoelectric modules for refrigeration is of great importance. Photovoltaic panels serve as a means to extract the energy from solar radiation and provide the needed electrical energy to power the modules ensuring cleaner source of energy, helps in reducing the dependence on non-renewable sources of energy, zero emissions thereby reducing the global warming effect and depletion of the ozone layer. The photovoltaic effect served as the driving principle in the development of solar panels and was discovered by Edmond Becquerel in 1839. He discovered that some materials produced electricity when exposed to solar radiation. They are made up of semiconductors which are mostly silicon based but not necessarily. As light hits the semiconductors on the PV cell, photons which possess energy smaller than the bandgap energy pass through the material. This bandgap energy is the energy required to free an electron from the pull of a covalent bond [9].

Table 1: Overview of the figure of merit of some materials [6]

Materials	Figure of Merit
PbTe	$1.2x10^{-3}$
PbSe	$1.3x10^{-3}$
Pb_2Te_3	$1.2x10^{-3}$
Bi_2Te_3	$1.3x10^{-3}$
$BiSb_2Te_3$	$3.3x10^{-3}$

Since the discovery of the Seebeck effect, Peltier effect and the basic principles underlying the operation of thermoelectric cooling; a lot of research has gone into the study and efficient development of thermoelectric cooling technology. There are many reports that characterize the inner workings of thermoelectric refrigerators and operation under various conditions. Raju et al [10] underscored the importance of using Peltier modules with an increased figure of merit in designing a thermoelectric cooling system. Their work indicated that thermoelectric material quality can have a pronounced effect on the overall performance of the refrigerator. They recorded a change in temperature of about 15°C of the inner refrigeration area of their fabricated solar thermoelectric refrigerator in the space of 50 minutes. They also obtained a

low COP of about 0.17 which is expected for most thermoelectric systems.

The problem of low COP observed in thermoelectric cooling systems was reiterated by Ghude et al [11]. They admitted the COP was low, about 0.6040 for their cooling system but argued that further research can bring out more improvement and that the quality of living and the value of human life should be of more concern. Shetty et al [12] conducted an experimental analysis of solar powered thermoelectric refrigerator, they developed a thermoelectric refrigerator that utilizes Peltier effect to cool the volume within two hours and provide retention of at least thirty minutes.

Chavan et al [13] highlighted the importance of a large current in causing a large temperature difference. Their design which utilized two Peltier modules had a value of 0.44 for the C.O.P. They were also able to experimentally show relations of C.O.P with current, power and temperature difference. For an increase in current of 4.5A, there was a corresponding C.O.P increase up to a certain value before decreasing. The experiments also highlighted a C.O.P decrease with increase in input power and C.O.P decrease with increase in temperature difference. Reddy and Basha [14], designed a system specifically for preservation of medicines and vaccines in flood affected areas where there is little or no power supply. They used solar panels to charge a lead acid battery and connected it to a Peltier thermoelectric device. Their device absorbed 312 J of heat in a second. On a fully sunny day, the electrical energy conversion from the photovoltaic cells was calculated by them to be 4 amps per hour.

Kaushik et al [15] tried to experimentally evaluate the performance of a solar thermoelectric cooling system with a cold storage of 3-liter capacity. They were able to show experimentally that the temperature within the cold box could be maintained within a temperature of 10°C to 15°C. They were also able to relate graphically the cooling power of the solar system with respect to time, energy efficiency with solar radiation, and irreversibility of system with time. Their graphical illustration depicted higher cooling power towards mid-day, lower energy efficiency with increase in solar radiation, and higher irreversibility of system towards mid-day. Singh and Kumar [8] worked on the design of a thermoelectric solar refrigerator and simulated its performance using MATLAB. They were able to discover that the C.O.P which determined the effectiveness of the refrigerator's performance was dependent on the temperature between the heat source and sink. Dhawde et al [2] detailed out the types of refrigerators and offered their opinion, on why the use of a solar thermoelectric refrigerator, is a much more viable alternative to the traditional compression refrigerators. They opined that the thermoelectric refrigerator was eco-friendly, noiseless, clean and utilized a renewable source of energy in the light of the world's ongoing energy crisis. They also placed an average range for the C.O.P of thermoelectric refrigerators to be between 0.3-0.6.

Patond et al [3] fabricated a portable solar Peltier heating and cooling system. They also tested the device on different materials and discovered for substances like water, the effectiveness of its cooling rate via conduction was much higher than convection. This discovery strongly helps in the design of feasible thermoelectric refrigerator systems to effectively cool water and substances which are worse off than it. This present research gave a detailed design and stepwise development of a solar powered thermoelectric refrigerator which is lacking in the reviewed papers. This refrigerator uses twenty TEC1-12706 modules in pair of ten placed 180° apart for uniform cooling while monitoring the environmental conditions.

2. Governing Equations for Thermoelectric Cooling

2.1 Thermoelectric Cooler Modelling

Figure 3 shows a thermoelectric element with boundary conditions having cross-sectional area A_x and length, L. The Fourier heat flowing in at point x and x+Δx, is expressed as:

$$q_x = -k_e A_x \left[\frac{dT}{dx}\right]_x \quad (1)$$

$$q_{x+\Delta_x} = -k_e A_x \left[\frac{dT}{dx}\right]_{x+\Delta x'} \quad (2)$$

where k_e is thermal conductivity of element, $W.m^{-1}.K^{-1}$; A_x is the cross-sectional area of the thermoelectric couple, m^2; dT is the temperature gradient, K; dx is spatial difference, m; while q_x is Fourier heat at position x, W; $q_x+\Delta_x$ is the Fourier heat at position, x+Δx , W. The Joulean heat due to current flowing through a material is expressed as [16]:

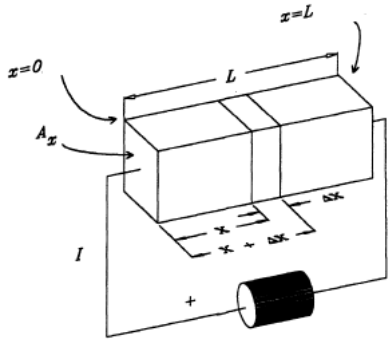

Figure 3: Thermoeletric element with Dirichlet boundary conditions [16]

$$q_j = \frac{I^2 \rho_r \Delta_x}{A_x} \tag{3}$$

where I is current, A;ρ_r is the resistivity of the element, Ωm. Using the concept of conservation of energy, then:

$$-k_e A_x \left[\frac{dT}{dx}\right]_{x+\Delta x} = -k_e A_x \left[\frac{dT}{dx}\right]_x + \frac{I^2 \rho_r \Delta x}{A_x} \tag{4}$$

Substituting equation (1), equation (2) and equation (3) into equation (4), yields:

$$-k_e A_x \left[\frac{dT}{dx}\right]_{x+\Delta x} = -k_e A_x \left[\frac{dT}{dx}\right]_x + \frac{I^2 \rho_r \Delta x}{A_x}$$

upon rearrangement gives

$$k_e A_x \left(\left[\frac{dT}{dx}\right]_{x+\Delta x} - \left[\frac{dT}{dx}\right]_x\right) + \frac{I^2 \rho_r \Delta x}{A_x} = 0$$

Dividing through by Δx and taking the limit of Δx →0, yields:

$$k_e A_x \frac{d^2T}{dx^2} + \frac{I^2 \rho_r}{A_x} = 0 \tag{5}$$

Equation (5) is a linear homogenous second order differential equation. Dividing Equation (5) through by $k_e A_x$ yields:

$$\frac{d^2T}{dx^2} + \frac{I^2 \rho_r}{k_e A_x^2} = 0$$

Integration of Equation (6) gives:

$$\frac{dT}{dx} + \frac{I^2 \rho r^x}{2k_e A_x^2} + C_1 = 0$$

Further integration yields:

$$T + \frac{I^2 \rho_r x^2}{2k_e A_x^2} + C_1 x + C_2 = 0 \tag{7}$$

Application of Dirichlet boundary conditions when x=0, T=T_h ; equation (7) can be expressed as:

$$T - T_h + \frac{I^2 \rho r^{x^2}}{2k_e A_x^2} + C_1 x = 0 \tag{8}$$

Application of Dirichlet boundary conditions when x = L, T=T_c; equation (6) can be expressed as:

$$T - T_h + \frac{I^2 \rho r L^2}{2k_e A_x^2} + C_1 L = 0 \tag{9}$$

In the light of equation (8) and equation (9), the temperature distribution in the thermoelectric material is readily expressed as:

$$T(x) = T_h - \left(\frac{I^2 \rho}{2k_e A_x^2}\right) x^2 - \left(\frac{Th - Tc}{L} - \frac{I^2 \rho L}{2k_e A_x^2}\right) x \tag{10}$$

Differentiation of equation (10) and equating to zero gives the position of highest temperature, let X indicates the position:

$$\frac{dT}{dx} = -\frac{I^2 \rho_r X}{k_e A_x^2} - \frac{Th - Tc}{L} + \frac{I^2 \rho_r L}{2k_e A_x^2} \tag{11}$$

Where X can be expressed as:

$$X = \frac{L}{2} - \frac{k_e dT A^2 x}{I^2 \rho_r L}$$

Equation (12) can be rearranged as:

$$X = L - L\left(\frac{1}{2} + \frac{k_e \Delta T A^2 x}{I^2 \rho_r L^2}\right) \tag{12}$$

Which can be further expressed as:

$$X = L - Lj$$

Where:

$$j = \frac{1}{2} + \frac{k_e \Delta T A_x^2}{I^2 \rho_r L^2} \tag{13}$$

j is known as the proportion of Joulean heat transferred to the cold junction and can also be expressed as:

$$j = \frac{1}{2} + \frac{k \Delta T}{I^2 R} \tag{14}$$

The resistance of the thermoelectric module can be expressed as:

$$R = \frac{\rho_p L_P}{A_p} + \frac{\rho_n L_n}{A_n} \tag{15}$$

While the thermal conductivity can be expressed as:

$$k = \frac{k_p L_p}{A_p} + \frac{k_n L_n}{A_n} \quad (16)$$

Where ρ_p, ρ_n are the electrical resistivity of p-type material and n-type material, Ω m; L_p , L_n are the length of p-type material and n-type material, m; A_p , A_n are the area of p-type material and area of n-type material, m^2; k_p , k_n are the thermal conductivity of p-type material and n-type material, $W.m^{-1}.K^{-1}$. The net heat absorbed at the cold junction equals the Peltier heat subtracted from the proportion of Joulean heat transferred to the cold junction. This can be expressed as:

$$q_c = \alpha I T_c - jI^2 R \quad (17)$$

Substituting equation (14) into equation (17) gives:

$$q_c = \alpha I T_c - \frac{I^2 R}{2} - k\Delta T \quad (18)$$

The initial expression for q_c had the Joulean effect $\frac{I^2R}{2}$subtracted from the Peltier heat. At the cold junction, this value would be added, hence, q_h which denotes heat dissipated at hot junction can be expressed as:

$$q_h = \alpha I T_h + \frac{I^2 R}{2} - k\Delta T \quad (19)$$

Where T_h is the temperature at the hot junction, K.

2.2 Cooling Loads

The total heat to be removed from the refrigerator chamber comprises heat transfer across the walls, products load and infiltration due to door opening. The heat transfer across the walls of the chamber can be expressed as [12]:

$$q = \frac{T_o - T_i}{R} \quad (20)$$

And the thermal resistance of the walls of the chamber can be expressed as:

$$R = \frac{1}{h_{outer\,air} A} + \frac{L_{formica}}{K_{formica} A} + \frac{L_{wood}}{K_{wood} A} + \frac{L_{formicainner}}{K_{formica} A} + \frac{1}{h_{innerair} A} \quad (21)$$

Where is the temperature of outer air, K; T_i is the temperature of inner air, K; $h_{outer\ air}$ is coefficient of heat transfer of outside air, $W.m^{-2}.K^{-1}$; $h_{inner\ air}$ is coefficient of heat transfer heat of inner air, $W.m^{-2}.K^{-1}$; $L_{formica}$ is length of outer Formica covering, m, $L_{formicainner}$ is length of inner Formica covering, m, is length of ply wood, m; $k_{formica}$ and k_{wood} represent the thermal conductivity of Formica and ply wood respectively with units of $W.m^{-2}.K^{-1}$. The heat dissipated by the mass being cooled is the product load and can be expressed as [17]:

$$Q_{active} = \frac{mC_p \Delta T_a}{\Delta t} \quad (22)$$

And

$$m = m_a + m_s \quad (23)$$

Where m_a is mass of air been cooled, kg and m_s is mass of substance been cooled, kg; C_p is the specific heat capacity of mass to be cooled, $kJ.kg^{-1}.K^{-1}$; Δt is time in which mass is cooled, s, and ΔT_a is the temperature difference of mass and inner cooling chamber, K. The heat due to Infiltration can be simply expressed as:

$$Q_{\inf iltration} = V\rho C_{pa}(T_i - T_o) \quad (24)$$

Where V is the volumetric air flow rate, $m^3.s^{-1}$; ρ is air density, $kg.m^{-3}$; C_{pa} is specific heat capacity of air, $kJ.kg^{-1}.K^{-1}$. The cooling load is a summation of equation (22), equation (23) and equation (24) expressed as:

$$Q_{cool} = Q_{active} + Q_{\inf iltration} + q \quad (25)$$

2.3 Coefficient of Performance of a Thermoelectric Cooler

The coefficient of performance, measures the effectiveness of the couples in transferring heat from an enclosed space, this dimensionless parameter can be expressed as [5]:

$$\eta = \frac{q_c}{p} \quad (26)$$

The power input to the thermocouples equals the difference between the heat transfer rates:

$$p = q_h - q_c \quad (27)$$

Substituting Equation (19) and equation (18) into Equation (27) gives the power consumed by the couples as:

$$P = \alpha I \Delta T + I^2 R \quad (28)$$

Substitution of Equation (18) and Equation (28) into equation (26) yields the coefficient of performance as:

$$\eta = \frac{\alpha I T_c - \frac{I^2 R}{2} - k\Delta T}{\alpha I \Delta T + I^2 R} \quad (29)$$

For maximum cooling effect, the current required can be obtained by differentiating equation (18) with respect to and equating to zero to yield:

$$\frac{dq_c}{dI} = \alpha T_c - IR = 0$$

Where the maximum current is obtained from the relation:

$$I_m = \frac{\alpha T_c}{R} \tag{30}$$

Substituting equation (30) into equation (18) gives the maximum cooling effect as:

$$q_{cm} = \frac{\alpha^2 T_c^2}{2R} - k\Delta T \tag{31}$$

From equation (31) the maximum temperature difference can be expressed as:

$$\Delta T_m = \frac{\alpha^2 T_c^2}{2kR} \tag{32}$$

Equation (31) can be re-expressed as:

$$q_{cm} = \frac{\alpha^2 k T_c^2}{2kR} - k\Delta T \tag{33}$$

Substituting equation (32) into equation (33) yields:

$$q_{cm} = k\Delta T_m \left(1 - \frac{\Delta T}{\Delta T_m}\right) \tag{34}$$

Substituting equation (30) and equation (32) into equation (28) gives the maximum power for maximum cooling as:

$$P_m = 2k\Delta T_m \left(1 + \frac{\Delta T}{T_c}\right) \tag{35}$$

Substituting equation (34) and equation (35) into equation (26) gives the coefficient of performance for maximum cooling effect as:

$$\eta_{cm} = \frac{1 - \Delta T / \Delta Tm}{2(1 + \Delta T / T_c)} \tag{36}$$

For n couples in a module, α , (R)n , and (k)n can be approximated as [5]:

$$\alpha = \frac{V_{\max}}{T_h} \tag{37}$$

$$(R)n = \frac{T_h - \Delta T_{\max}}{T_h} \frac{V_{\max}}{I_{\max}} \tag{38}$$

$$(k)n = \frac{T_h - \Delta T_{\max}}{2\Delta T_{\max}} \frac{V_{\max} \mathrm{I}_{\max}}{T_h} \tag{39}$$

Where V_{max} is maximum voltage when no heat is absorbed at cold junction, V; I_{max} is maximum current when no heat is absorbed at cold junction, A; ΔT_{max} is maximum temperature difference when no heat is absorbed at cold junction, K.

2.4 Photovoltaic Cell Models

Figure 4 form the basis of analysis of a PV cell. A PV cell can be taken to be an equivalent circuit made up of one diode, resistance in series, R_s and resistance in parallel, R_p.

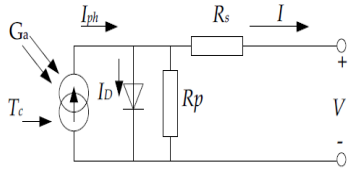

Figure 4: Equivalent circuit for a single PV cell [18]

The effect of the parallel resistance, R_p, can be considered trivial and insignificant because the current through it is less compared to others. The output current of the PV cell is [18]:

$$I = I_{ph} - I_0 \left(e^{\frac{q_{ch}(V_c + IR_s)}{ak_bT}} - 1 \right) - \frac{V_c + IR_s}{R_p} \tag{40}$$

Where I_{ph} is the photocurrent, A; I_0 is the diode saturation or reverse saturation current, A; q_{ch} is the electron charge C; k_b is the Boltzmann constant $J.K^{-1}$; T is the operating temperature, K; a is the diode factor, R_s is the series resistance, Ω; R_p is the shunt resistance, Ω; V_c is the cell voltage, V. The photocurrent and reverse saturation current are dependent on temperature and is expressed as [19]:

$$I_{ph} = (I_{ph})_{T_1} + K_0(T - T_1) \tag{41}$$

Where T_1 is the reference temperature of a PV cell and K_0 is some constant. Also

$$(I_{ph})_{T_1} = (I_{sc})_{T_1} \frac{G}{G_{STC}} \tag{42}$$

And

$$K_0 = \frac{(I_{sc})_{T_2} - (I_{sc})_{T_1}}{T_2 - T_1} \tag{43}$$

G is the Irradiance, $W.m^{-2}$; G_{STC} is the Irradiance, $W.m^{-2}$ at standard temperature condition and I_{SC} is the short circuit current, A. The reverse saturation current or diode saturation current is dependent on temperature and can be obtained from the relation [19]:

$$I_0 = (I_0)_{T_1} \left(\frac{T}{T_1}\right)^{\frac{s}{a}} e^{\frac{q_{ch}(E_g)_{T_1}\left(\frac{1}{T} - \frac{1}{T_1}\right)}{ak_b}} \tag{44}$$

Where E_g is the silicon gap energy of the semiconductor, J . While

$$(I_0)_{T_1} = \frac{(I_{sc})_{T_1}}{\left(e^{\frac{q_{ch}(V_{oc})T_1}{ak_bT_1}} - 1\right)} \quad (45)$$

If the parallel resistance were considered, then [20]:

$$(I_0)_{T_1} = \frac{(I_{sc})_{T_1}}{\left(e^{\frac{q_{ch}(V_{oc})T_1}{ak_bT_1}} - 1\right)} + \frac{V_{oc}}{R_p} \quad (46)$$

Where V_{oc} is the open circuit voltage, V. The value of series resistance can also be expressed as [18]:

$$R_s = -\left(\frac{dV_c}{dI}\right)_{V_{oc}} - \frac{\frac{ak_bT}{q}}{(I_o)_{T_1 e}\frac{q_{ch}v_{oc}T}{ak_bT}} \quad (47)$$

Where $\left(\frac{dV_c}{dI}\right)_{V_{oc}}$ is the slope of the I-V curve at V_{OC}. The series resistance and parallel resistance can be approximated as [20]:

$$R_s = 0.015\frac{P_{\max}}{(1mp)^2} \quad (48)$$

And

$$R_p = \frac{\left(V_{mp} + I_{mp}R_S\right)^2}{0.015 \times P_{\max}} \quad (49)$$

Where I_{mp} is the current at maximal power point, A; P_{max} is the maximum power, W; V_{mp} is the voltage at maximal power point, V. The model of the PV cell is obtained using recursive equation to obtain the cell current as [18]:

$$I_{n+1} = I_n - \frac{I_{ph} - I_n - I_0\left(e^{\frac{q_{ch}(V_c + I_nR_s)}{ak_bT}} - 1\right)}{-1 - I_o\left(\frac{q_cR_s}{ak_bT}\right)\left(e^{\frac{q_{ch}(V_c + I_nR_s)}{ak_bT}}\right)} \quad (50)$$

2.5 Model of a Photovoltaic Module

A PV module consist of PV cells connected electrically in series or parallel and mounted on some structure. For series configuration the PV module is the current is expressed as [18]:

$$I = I_{ph} - I_0\left(e^{\frac{q_{ch}(V_c + IR_s)}{N_s ak_bT}} - 1\right) - \frac{Vc + IR_s}{R_p} \quad (51)$$

where N_s is number of cells in series. The thermal voltage of the module can also be expressed as [18]:

$$V_t = \frac{N_s k_b T}{q_{ch}} \quad (52)$$

The photocurrent is temperature-dependent expressed as [18]:

$$I_{ph} = \left(I_{ph}\right)_{T1} + K_i\Delta T\frac{G}{G_{STC}} \quad (53)$$

Where K_i is temperature coefficient current, A.K-1; ΔT is the temperature variation, K. The diode saturation current's dependence on temperature for the module can be related as [18]:

$$I_0 = (I_0)_{T_1}\left(\frac{T}{T_1}\right)^3 e^{\frac{q_{ch}(Eg)_{T_1}}{ak_b}\left(\frac{1}{T}\frac{1}{T_1}\right)} \quad (54)$$

Where

$$(I_0)_{T1} = \frac{(I_{sc})T_1}{\left(\frac{(C_{oc})T_1}{e^{a(V_t)T_1} - 1}\right)} \quad (55)$$

Figure 5 shows an equivalent series and parallel arrangement of PV cells in a module.

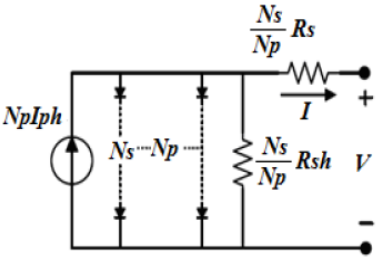

Figure 5: Equivalent circuit for a PV array [21]

The I-V characteristics of a PV module or panel involving N_p parallel strings and N_s series cells in each string is obtained by modification of equation (51) to yield give [21]:

$$I = N_pI_{ph} - N_pI_0\left(e^{\frac{v}{\frac{N_s}{N_p}} + \frac{1K_s}{V_T}} - 1\right) - \frac{\frac{VN_p}{N_s} + IR_s}{R_p} \quad (56)$$

Where is terminal voltage, V; is same as known as the shunt or parallel resistance, Ω. The ratio of maximum power to be delivered to the product of open-circuit voltage and short-circuit current is termed fill factor. It can be expressed as [15]:

$$FF = \frac{V_{mp}I_{mp}}{V_{oc}I_{sc}} \quad (57)$$

The short circuit current is expressed as:

$$I_{sc} = I_{ph} - I_0\left(e^{\frac{I_{sc}K_s}{N_s V_T}} - 1\right) - \frac{I_{sc}R_s}{R_p} \quad (58)$$

And

$$I_{mp} = I_{ph} - I_0\left(e^{\frac{V_{mp}+I_{mp}K_s}{N_s V_T}} - 1\right) - \frac{V_{mp}+I_{mp}R_s}{R_p} \quad (59)$$

The minimum number of solar panels required for the thermoelectric cooler module is obtained as [22]:

$$n_p = \frac{1.3Lh}{W_p PGF} \quad (60)$$

Where L is the thermoelectric cooler modules, W, h is the operating hours, W_p is the panel peak rating and PGF stand for power generation factor. According to Da Roza and Ordonex, [23], the number of panels required can be estimated using the relation:

$$n_p = \frac{Lh}{S_h W_p \eta_{sys}} \quad (61)$$

Where S_h is sunshine hours per day and is the system efficiency. In order to protect the batteries, an appropriate solar charge controller must be sized to match the PV array and batteries. The charge controller rating is gotten using the expressions [24]:

$$CC_r = 1.3 I_{sc} N_s \quad (62)$$

$$I_{sc} = \frac{1.25 n_p W_p}{B_v} \quad (63)$$

Where I_{SC} is the short circuit current, A, and B_v is the battery nominal voltage, V. The required number of batteries for the installation is given as [25]:

$$n_b = \frac{1.3L \times h \times DOA}{DOD \times B_v \times B_r'} \quad (64)$$

where DOA stand for days of autonomy. DOD stand for depth of discharge, ξ_b is the battery efficiency and B_r is the battery rating, AH. Whenever electricity is conducted through a wire, energy is lost and there will be a voltage lost. Selecting the correct size and type of wire enhance the performance and thus the reliability of the system. According to Anyanime et al, [26], the maximum current passing through the wire is:

$$\mathrm{I}_{\max} = N_p \times I_{sc} \times FOS \quad (65)$$

where N_p is the number of modules in parallel, FOS stand for factor of safety. The cross-sectional area of the required cable is:

$$A = \frac{\rho L_w I_{\max}}{V_d} \quad (66)$$

where ρ is the resistivity of wire, Ωm; L_w is the length of wire, m, V_d is the voltage drop, V, taken to be 0.04 of the operating voltage.

3. Research Methodology

This research focused on design and experimental testing of a solar powered thermoelectric refrigerator. The design of the refrigeration cooling chamber and its components was made using the FREECAD software. Figure 6 shows the 3-D drawing of the refrigerator chamber and associated components with its orthogonal views.

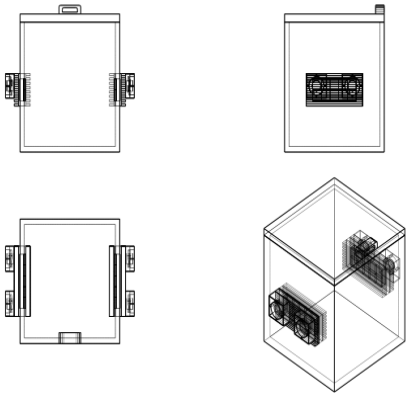

Figure 6: Design of the thermoelectric refrigerator

Figure 7: Assembled TEC1-12706 Thermoelectric Modules

Mathematical models of the thermoelectric refrigerator and PV cells were carried out and solved using MATLAB SIMULINK, to depict the performance of the thermoelectric refrigerator at various operating conditions. Thereafter the thermoelectric generator was constructed using twenty TEC 1-12706 thermoelectric modules in pairs of ten and attached to the heat-sink using thermal paste as shown in figure 7.

The experimental setup consists of the thermoelectric refrigerator chamber, three 100 AH storage batteries, and two 150W PV panels with 30 A charge controller, MTM-380 SD three channel temperature logger, 8706 digital psychrometer and TM-206 solar meter as shown in figure 8.

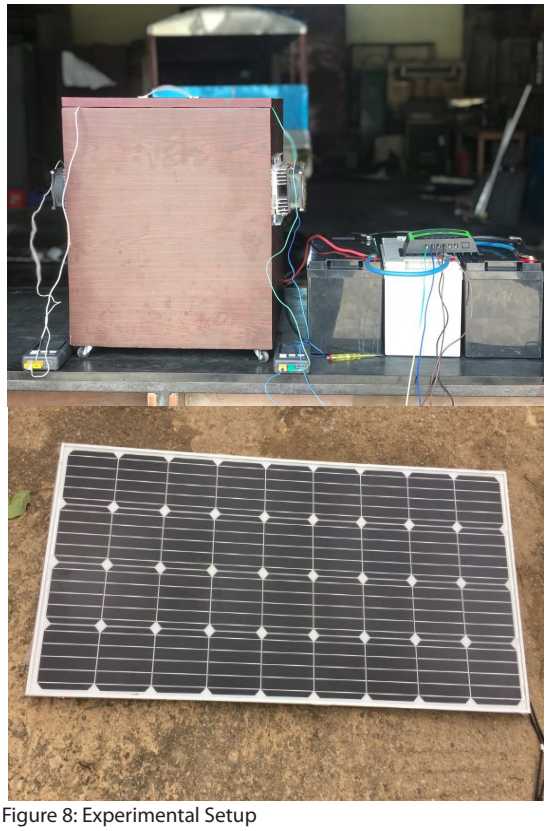

Figure 8: Experimental Setup

4. Results and Discussion

4.1 Heat absorbed at Cold Junction with Voltage at different Temperature Gradients

Figure 9 shows plot of heat absorbed with voltage at different temperature gradients. It is clear from the graph that as current increases, the cooling effect increases. The quantity of heat absorbed from the refrigerated chamber increases with an increase in voltage and decreases with an increase in temperature gradients. This can be attributed to irreversibility cause transmission of heat with large temperature differences. Hence it is efficient to allow system operate at a moderate temperature range for a particular voltage value. The expected heat pumping capacities of the TEC1-12706 module are 42.6W, 38.9W, 35.3W and 31.7W at temperature gradients of 5°C, 10°C, 15°C and 20°C respectively.

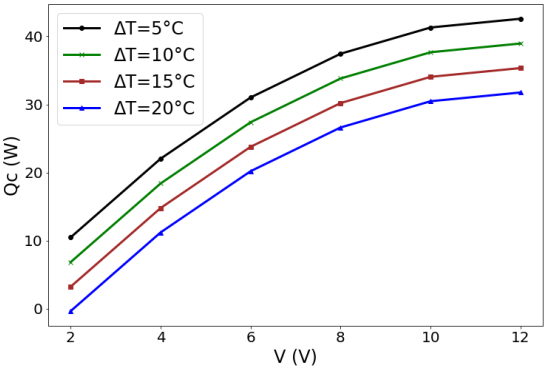

Figure 9: Heat absorbed vs Voltage

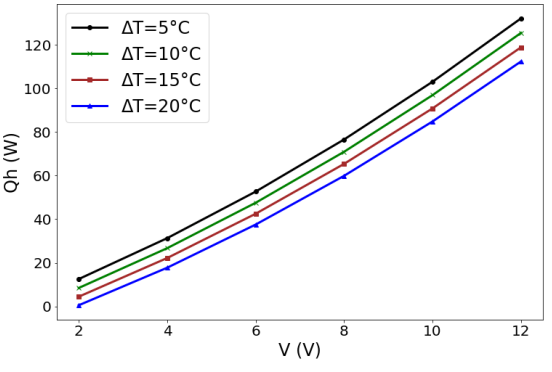

Figure 10: Heat Dissipation vs Voltage

4.2 Heat Dissipation at Hot Junction with Voltage at different Temperature Gradients

Figure 10 shows the variation of heat dissipation with voltage at different temperature gradients. The dissipated heat to the environment shows a near linear relation to voltage but inversely proportional to the temperature gradients, due to an increase in Peltier effect. As expected of a refrigeration system for all position of voltage and temperature gradient, the heat dissipation is always greater than the heat absorbed. The expected heat dissipation capacities of the TEC1-12706 module are 132W, 125.3W, 118.7W and 112.2W at temperature gradients of 5°C, 10°C, 15°C and 20°C respectively.

4.3 Coefficient of Performance with Voltage at different Temperature Gradients

Figure 11 shows plot of coefficient of performance, COP, against voltage at various temperature gradients. At greater temperature gradients the COP is first seen to increase, peak and then decreases with an increase in temperature gradient and decreases with an increase in voltage. The profile visibly tends to converge and at lower temperature gradient the curves tend to flatten out, this can be verified with the work of Huang et al [27]. The expected COP capacities of the TEC1-12706 module are 0.468, 0.436, 0.402 and 0.368 at temperature gradients of 5°C, 10°C, 15°C and 20°C respectively.

4.4 Variation of Current with Voltage at different Insolation Rates

Figure 12 depicts the current voltage characteristic of a photovoltaic cell at different insolation. The profile of the curves reveal that as the solar irradiance that falls on the PV cells increases, the current and voltage output of the cell also increase which is as a result of an increase in the electron-hole pairs formed in the semiconductor, this can be verified using the work of Tyagi et al, [28] and Tamarakar et al, [19].

4.5 Variation of Current with Voltage at different Cell Temperatures

Figure 13 shows the graphical relationship of current with voltage at different cell temperatures. As the cell temperature increases, both the current and voltage are seen to decrease. This is due to the shrinkage of the band gap as temperature increases, causing the open circuit voltage to drop as reported also by Mahmood and Selman [21] and Tyagi et al [28].

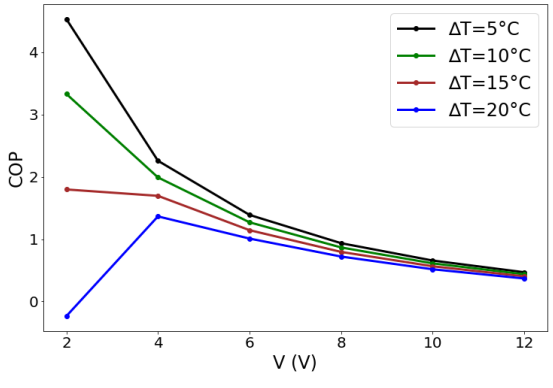

Figure 11: C.O.P vs Current

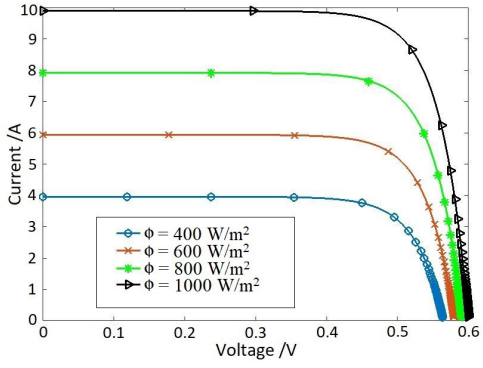

Figure 12: Current and voltage Profile of PV cell at various Irradiation

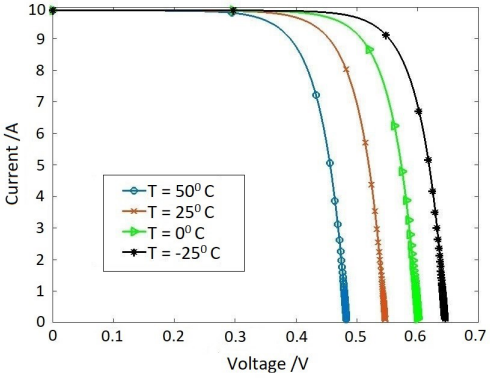

Figure 13: Current and voltage Profile of PV cell at various Cell Temperatures

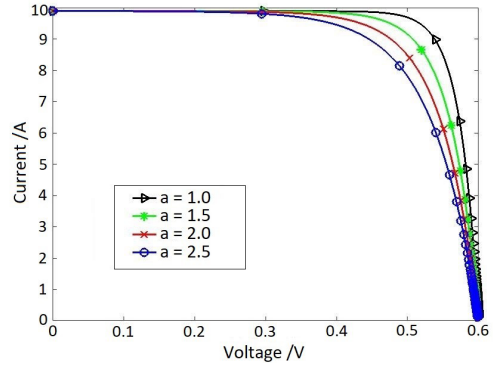

Figure 14: Current and voltage Profile of PV cell at various Ideality Factor

4.6 Variation of Current with Voltage at different Ideality Factors

Figure 14 shows the graphical relation of current with voltage at different ideality factors. As the ideality factor increases, the current and voltage output reduces. The effect of the ideality factor on the cell performance is quite negligible at lower

voltages but becomes significant as voltages increases a trend also reported by Tamarakar et al [19] and Das, [29].

4.7 Variation of Current with Voltage at different Values of Series Resistance

Figure 15 is a plot of current and voltage characteristics of PV cell at different values of series resistance. As the series resistance increases, the current generated drops at the same open circuit voltage. The series resistance acts as a barrier to current flow, therefore, in order to maximize power extraction from a solar cell, series resistance should be kept to a minimum, similar results were obtained by Singh and Kumar [8] and Tamarakar [19].

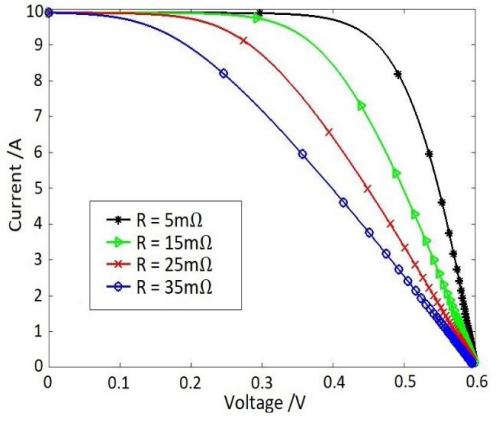

Figure 15: Current and voltage Profile of PV cell at various Series Resistance

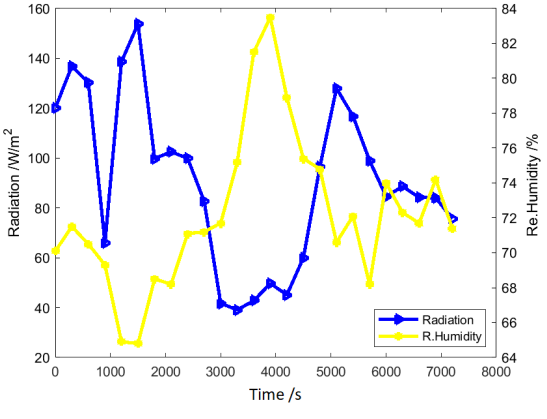

Figure 16: Solar Irradiation and Relative Humidity with time

4.8 Experimental Plots

4.8.1 Atmospheric Condition

Figure 16 showed plots of solar irradiation and relative humidity of the environment during the experiment. As seen in the plots the solar irradiation and relative humidity are dynamic in nature as expected which will in turn influence the performance of the PV cell. The storage batteries thus tend to smoothen out the operation of the thermoelectric refrigeration maintaining it at a constant voltage of 12 V. Figure 17 capture the variation in the dry and wet bulb temperatures also clearly seen to be dynamic.

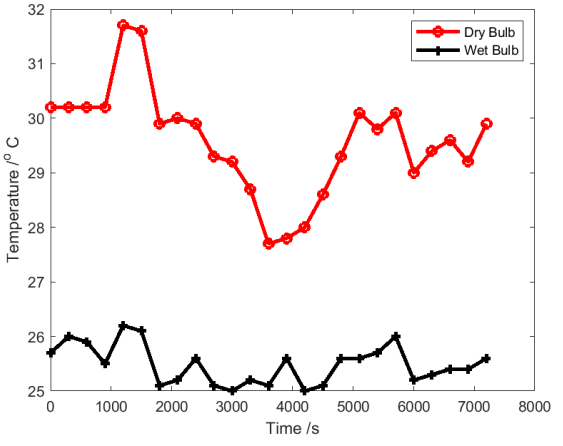

Figure 17: Dry and Wet Bulb Temperatures with Time

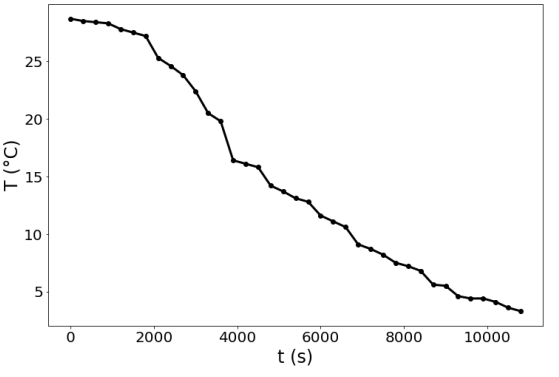

Figure 18: Cooler Temperature with Time

4.8.2 Cooler Temperature against Time

Figure 18 showed the relationship between the temperature of the refrigerated chamber and time during actual test of the thermoelectric refrigerator. The temperature decreased on a relatively steady rate from 28.7°C to 3.3°C in a space of three hours. It was not noticeably affected by the variations in the atmospheric conditions due to action of storage batteries in the installation.

5. Conclusion

A solar powered thermoelectric refrigerator was modelled, designed and tested with the potential to effectively cool objects efficiently in an eco-friendly way. The design of the refrigeration cooling chamber

and its components was made using the FREECAD software while the models were solved using MATLAB. Simulation results of the thermoelectric refrigeration showed the heat pumping capacities of the TEC1-12706 module as 42.6W, 38.9W, 35.3W and 31.7W at temperature gradients of 5oC, 10oC, 15oC and 20oC respectively, the heat dissipation capacities of the TEC1-12706 module as 132W, 125.3W, 118.7W and 112.2W at temperature gradients of 5°C, 10°C, 15°C and 20°C respectively and the corresponding coefficient of performance as 0.468, 0.436, 0.402 and 0.368 at temperature gradients of 5°C, 10°C, 15°C and 20°C respectively. The experimental results indicated a steady decline of temperature in the refrigerated chamber from 28.7oC to 3.3°C in a time frame of three hours. Solar power thermoelectric refrigerator is an alternative source of cooling as it is environmentally friendly, development of multi stage modules can greatly improve the efficiency and give very effective performance of thermoelectric refrigerators.

References

[1.] Chen L.Y., Chien, J. Z., Lee S. W., Jwo S. C., Cho C. K. (2014). Experimental Investigation on Thermoelectric Chiller Driven by Solar Cell. International Journal of Photoenergy, pp. 1-8.

[2.] Dhawde B. M., Mourya E., Yadav A., Samuel D., Mohod A. S., Deshpande N. V. (2015). Review on Portable Solar Thermoelectric Refrigeration Air cum Cooler. International Journal of Advance Research and Engineering, 4(10), pp.44-58.

[3.] Patond B. S., Bhadake G. P., Patond B. C., (2015). Experimental Analysis of Solar Operated Thermo-Electric Heating and Cooling System. International Journal of Engineering Trends and Technology, 20(3), pp.125-130.

[4.] Jibhakate M. B., Nikose J., Mishra A., Khandare S., Choudhari S. (2016). Fabrication of Solar Operated Thermoelectric Refrigerator Cum Oven – a Review. International Journal for Research in Technological Studies, 3(4).

[5.] Rawat K. M., Sen K. P., Chattopadyhay H., Neogi S., (2013). Developmental and Experimental Study of Solar Powered Thermoelectric Refrigeration System. International Journal of Engineering Research and Applications, 3(4), pp.2543-2547.

[6.] Elmaaref, M. M. A., Askalany A. A., Salem M., (2015). Solar Thermoelectric Cooling Technology. Proceedings of 3rd International Conference on Energy Engineering, Faculty of Energy Engineering-Aswan University - Aswan – Egypt, December 28-30, 2015. Egypt: pp.1-7.

[7.] Raju A., Ajeesh J., Akash S., Akhil T. J., Bose V., Jinshah B. S., (2016). Devolopment of Portable Solar Thermoelectric Refrigerator. International Journal of Scientific and Engineering Research, 7(4), pp. 426-428.

[8.] Singh K. S., Kumar A., (2015). Thermoelectric Solar Refrigerator. International Journal for innovative research in science and technology, 1(9), pp.167-170.

[9.] Thedeby A. (2014). Heating and Cooling with Solar Powered Peltier Elements. Master's thesis, Department. of Energy Planning, Lund University.

[10.] Raju, A. , Ajeesh, J. , Akash, S. , Akhil, T.J. , Bose, V. , and Jinshah, B.S. , (2016). Devolopment of Portable Solar Thermoelectric Refrigerator. International Journal of Scientific & Engineering Research, 7(4), pp.426-428.

[11.] Ghude, A. A. , Belokar, V.N. , Deshmukh A., Tahokar A., Dande A., Monde L., Gosavi, G .D. (2014). Design, Analysis and Fabrication of Thermoelectric Solar Air Conditioning System. International journal of mechanical engineering and robotics research, 3(2), pp.399-403.

[12.] Shetty N., Soni L., Manjunath S., Rathi G., (2016). Experimental Analysis of Solar powered Thermoelectric Refrigerator. International Journal of Mechanical and Production Engineering, 4(8), pp.99-102.

[13.] Chavan D. S., Pawar S. V., Dhamal M. S., Kute S. K., Borade P. B., Dhumal G. S. (2015). Thermoelectric refrigeration system running on solar energy. International Journal of Recent Research in Civil and Mechanical Engineering, 2(1), pp.140-148.

[14.] Reddy M. K., Basha M. U., (2015). Solar Based Medicine Refrigerator. Journal of Advancement in Engineering and Technology, 3(2),pp.1-4.

[15.] Kaushik S. C., Hans R., Manikandan S., (2016). Theoretical and Experimental Investigations on Solar Photovoltaic Driven Thermoelectric Cooler System for Cold Storage Application. International Journal of Environmental Science and Development, 7(8), pp.615-620.

[16.] Clifton W. E., (1992). Thermoelectric Cooler Design. Master's thesis, Department. of Astronautical Engineering, Naval Postgraduate School.

[17.] Rawat K. M., Chattopadyhay H., Negoi S., (2013). A Review on Developments of Thermoelectric Refrigeration and Air Conditioning Systems: A Novel Potential Green Refrigeration and Air Conditioning Technology. International Journal of Emerging Technology and Advanced Engineering, 3(3), pp.362-367.

[18.] Rakotomananandro F. F., (2011). Study of Photovoltaic System. Master's thesis, Department of Electrical and Computer Science, Ohio State University.

[19.] Tamarakar V., Gupta S. C., Sawle Y., (2015). Single-Diode PV Cell Modeling and Study of Characteristics of Single and Two-Diode Equivalent Circuit. An International Journal

(ELELIJ), 4(3), pp.13-24.

[20.] Iyer S. V., (2017). Simulation of a Solar Photovoltaic Panel. Viewed 2 September 2018. http://www.pythonpowerelectronics.com/contents/tutorials/tutorial3/pvpanel_tutorial.pdf

[21.] Mahmood J. R., and Selman, N. H., (2016). Four MATLAB-Simulink models of photovoltaic system. International Journal of Energy and Environment, 7(5), pp.417-426.

[22.] Hemakshi B., Gaurang S. (2014). An Analysis of One MW Photovoltaic Power Plant Design. International Journal of Advanced Research in Electrical, Electronics and Instrumentation Engineering, 3(1), pp. 6969-6973.

[23.] Da Rosa A. V., Ordonez J. C., (2005). Fundamentals of Renewable Energy Processes. Fourth Edition, Elsevier Academic Press.

[24.] Sakiliba S. K., Hassan A. S. (2020). A Case Study for Solar PV Powered Cooling System in Lagos, Nigeria. Institute of Electrical and Electronic Engineers PES/IAS pp. 1-5.

[25.] Sakiliba S. K., Hassan A. S., Wu J., Sanneh E. S., Ademi S. (2015). Assessment of Stand-Alone Residential Solar Photovoltaic Application in Sub-Saharan Africa: A Case Study of Gambia. Journal of Renewable Energy, Vol. 2015, Article ID 640327. pp. 10.

[26.] Anyanime T. U., Emmanuel A. U., Mbetobong U. F. (2016). Design of Stand Alone Floating PV System for Ibeno Health Centre. Science Journal of Energy Engineering, 4(6), 2016, pp. 56-61.

[27.] Huang B. J., Chin C. J., DuANG C. L. (2000). A Design Method of Thermoelectric Cooler. International Journal of Refrigeration, 23, pp. 208-218.

[28.] Tyagi V. V., Rahim N. A. A., Rahim N. A., Selvaraj J. A. (2013). Progress in solar PV technology: Research and achievement. Renewable and Sustainable Energy Reviews, 20, pp. 443-461.

[29.] Das S. (2018). Design and implementation of MATLAB-Simulink Based Solar Cell Modelling and PV System Design Exercises for Advanced Student Learning. ASEE Annual Conference and Exposition.